

Dispersions of Non-Covalently Functionalized Graphene with Minimal Stabilizer

Dorsa Parviz,[†] Sriya Das,[†] H. S. Tanvir Ahmed,[‡] Fahmida Irin,[†] Sanjoy Bhattacharia,[†] and Micah J. Green^{†,*}

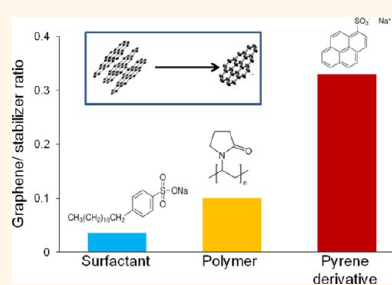
[†]Department of Chemical Engineering, Texas Tech University, Lubbock, Texas 79409, United States and [‡]Department of Mechanical Engineering, Texas Tech University, Lubbock, Texas 79409, United States

Graphene is a two-dimensional allotrope of carbon with a unique combination of electrical conductivity, mechanical strength, and high surface area.^{1,2} These remarkable properties make it a promising additive for a wide range of applications, many of which require scalable production of single- to few-layer graphene. Liquid phase exfoliation methods have been used broadly to produce colloidal suspensions of graphene due to their scalability and versatility for a wide range of applications, including polymer composites,^{3,4} conductive thin films,^{5,6} aerogels,^{7,8} solar cells,^{9–11} and inkjet printing.^{12–15} This method involves the exfoliation of graphene from a graphite source and dispersion in a solvent. However, this process is problematic because graphene layers tend to aggregate and restack due to strong intersheet van der Waals forces in order to minimize surface free energy.^{1,16} To overcome this problem, the graphene surface must be altered (either covalently through functionalization or noncovalently through stabilization), as discussed below, or dispersed in graphene-specific solvents.¹⁷

The most common liquid phase exfoliation technique involves the oxidation of graphite followed by exfoliation in water to yield single-layer graphene oxide (GO), which is marked by epoxide, –OH, and –COOH groups.^{18,19} GO is electrically insulating, so chemical and thermal methods are frequently used to reduce GO; however, the structure and electrical properties of reduced GO (RGO) are never fully restored to those of pristine graphene.^{6,20,21} Furthermore, Rourke *et al.* recently reported that GO on its own is not soluble in water; instead, it is stabilized by anomalous oxidative debris.²² Even so, the issue of GO solubility remains in question, given the conflicting literature on this point.²³

With these difficulties in mind, it is desirable to exfoliate and disperse pristine,

ABSTRACT We demonstrate that functionalized pyrene derivatives effectively stabilize single- and few-layer graphene flakes in aqueous dispersions. The graphene/stabilizer yield obtained by this method is exceptionally high relative to conventional nanomaterial stabilizers such as surfactants or poly-



mers. The mechanism of stabilization by pyrene derivatives is investigated by studying the effects of various parameters on dispersed graphene concentration and stability; these parameters include stabilizer concentration, initial graphite concentration, solution pH, and type and number of functional groups and counterions. The effectiveness of the pyrene derivatives is pH-tunable, as measured by zeta potential, and is also a function of the number of functional groups, the electronegativity of the functional group, the counterion, the relative polarity between stabilizer and solvent, and the distance from the functional group to the basal plane. Even if the dispersion is destabilized by extreme pH or lyophilization, the graphene does not aggregate because the stabilizer remains adsorbed on the surface. These dispersions also show promise for applications in graphene/polymer nanocomposites (examined in this paper), organic solar cells, conductive films, and inkjet-printed electronic devices.

KEYWORDS: graphene · pyrene derivative · π – π stacking · zeta potential · nanocomposite

unfunctionalized graphene. Although graphene may be exfoliated from graphite *via* sonication, dispersed pristine graphene suffers from the aggregation discussed above.¹⁶ However, in the presence of stabilizer molecules, surface free energy may be minimized by adsorption of stabilizers onto the graphene surface. Effective stabilizers include surfactants,^{24–27} certain polymers,^{28,29} and aromatic “ π – π stacking” molecules.³⁰ These stabilizers interact noncovalently with pristine graphene by surface adsorption, micelle formation, and/or π – π interaction; this noncovalent functionalization sterically or electrostatically prevents restacking of graphene sheets.^{29,31} However, to obtain dispersions with higher graphene concentrations, larger

* Address correspondence to micah.green@ttu.edu.

Received for review June 22, 2012 and accepted September 24, 2012.

Published online September 24, 2012
10.1021/nn302784m

© 2012 American Chemical Society

concentrations of polymers and surfactants are required; this results in excess stabilizer in the dispersion. In such dispersions, the low ratio of graphene to stabilizer concentration may hinder the use of the dispersion in composites, films, and electronic devices. The excess stabilizer may adversely affect the enhancement in mechanical and electrical properties of the graphene-loaded final product.

Such disadvantages necessitate the search for a new type of stabilizer that can efficiently stabilize a large amount of graphene at low concentrations. Polycyclic aromatic hydrocarbons (PAHs) show promise in this regard due to their π - π stacking interactions with graphene.³² Pyrene is a prominent example of PAHs, and functionalized pyrene derivatives have been reported by various groups to stabilize carbon nanotube and graphene dispersions.³³ Adsorption of these compounds onto the graphene surface occurs through π - π interactions between the planar surfaces of stabilizer and graphene and reduces the surface free energy of the dispersion. In these interactions both aromatic planar surfaces share the electrons of π -orbitals in a noncovalent bond.

For instance, An *et al.* prepared aqueous graphene dispersions using pyrenecarboxylic acid as stabilizer for sensor and ultracapacitor applications.³⁴ Similarly, Zhang *et al.* exfoliated single layers of graphene into an aqueous dispersion using pyrenetetrasulfonic acid sodium salt and aminomethylpyrene to fabricate transparent conductive films.³⁵ However, neither graphene yield nor dispersion effectiveness and stability were examined, and aggregates likely remained in these dispersions and final products. In other attempts to stabilize graphene through π - π stacking, Xu *et al.*, Su *et al.*, and Jang *et al.* used pyrenebutyrate and pyrenesulfonic acid sodium salt to stabilize graphene in water for use in electrochemical, solar cell, and composite applications.³⁶⁻³⁸ However, in their studies, RGO was initially prepared from GO and then stabilized in water. In summary, the prior literature lacks a comprehensive study of the parameters that control the effectiveness of pyrene derivatives in stabilizing graphene in solution.

In the present paper, we establish a detailed study of the application of pyrene derivatives as stabilizers for pristine graphene. Using various pyrene derivatives and varying the solution parameters, we evaluated the impact of stabilizer concentration, functional groups, counterions, and pH on dispersion quality, and we were able to prepare dispersions with exceptionally high graphene/stabilizer yields. We demonstrate that their molecular structure affects the formation and strength of π - π interactions, which determines the dispersed graphene yield.

RESULTS AND DISCUSSION

Dispersed Graphene Yield. We primarily demonstrate that a range of pyrene derivatives are able to effectively

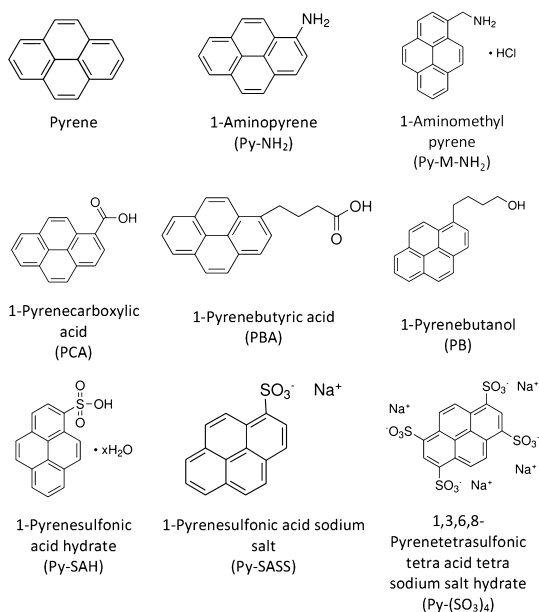


Figure 1. Chemical structure of the pyrene derivatives used in this study with their names and corresponding acronyms as used in the text.

stabilize graphene in water. The molecular structure of all investigated stabilizers is shown in Figure 1. These small molecules combine various functional groups with pyrene as the aromatic basal plane. To confirm the presence of single- to few-layer stabilized graphene in the dispersions, the Py-SASS-stabilized graphene samples were characterized using HRTEM; counting the number of folds at the edge of a graphene sheet in HRTEM images is a commonly used technique for characterizing the number of layers.^{29,39,40} A HRTEM image of a Py-SASS-stabilized graphene sheet is shown in Figure 2. The edge count of the graphene sheets reveals that the Py-SASS-stabilized graphene is 2–4 layers thick, as commonly observed in sonicated and centrifuged samples. These observations confirm our claim that we have successfully stabilized few-layer graphene. Additional TEM images along with lateral size of the Py-SASS-stabilized graphene sheets are shown in the Supporting Information (Figure S1).

The post-centrifugation graphene concentration in the dispersion is the main indicator of stabilizer effectiveness. To investigate the mechanism of stabilization, the post-centrifugation graphene concentrations are compared in Figure 3 and Figure S2 for pyrene derivatives with different initial stabilizer concentrations. The graphene concentration was calculated from the absorbance spectra. Pyrene, P-NH₂, and PB were insoluble in water, whereas other structures were dissolved in water either by heating or by pH changes. A similar trend is observed for all pyrene derivatives, where the final concentration of graphene initially increases with the addition of stabilizer and then decreases or remains constant. Py-SAH and Py-M-NH₂ became partially insoluble in water above their saturation concentration.

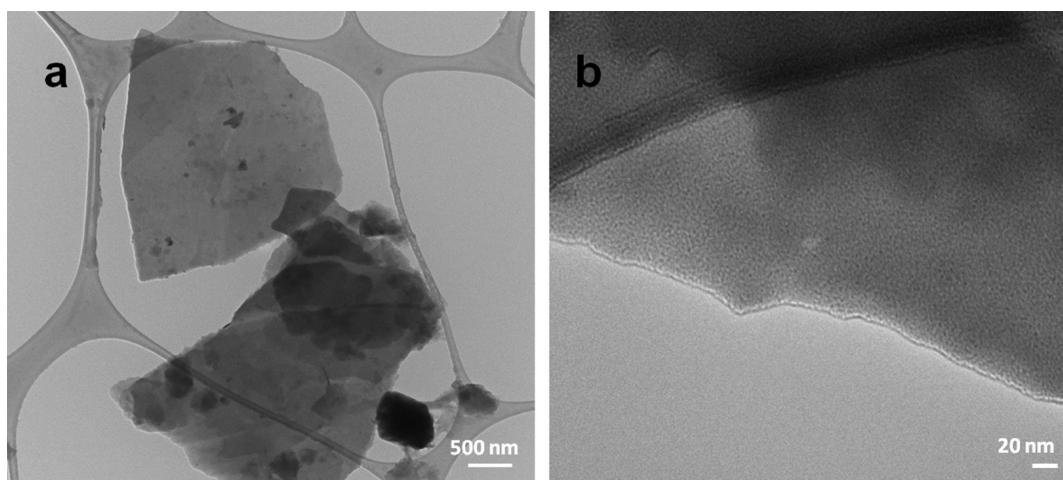


Figure 2. TEM images of stabilized graphene layers in a Py-SASS/graphene dispersion. (a) The lateral size of graphene sheets is about 2–2.5 μm , and (b) the edges of the sheets indicate that the dispersion contains single- to few-layer graphene as expected.

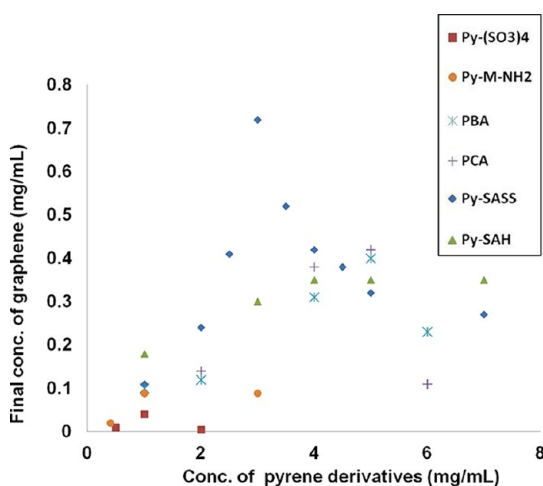


Figure 3. Final concentration of graphene for different pyrene derivatives. Initial concentration of expanded graphite in all samples is 20 mg/mL. Error bars are included in Figure S2 in the Supporting Information.

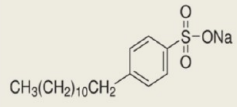
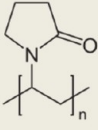
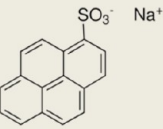
In this situation, excess stabilizer precipitates and cannot interact with graphene sheets. Therefore, in these samples the graphene concentration remained constant beyond the stabilizer solubility limit. However, in the case of Py-SASS, Py-(SO₃)₄, PBA, and PCA, the graphene concentration goes through a maximum as the stabilizer concentration is increased.

The change of zeta potential with stabilizer concentration for Py-SASS-stabilized samples is given in Figure S3. Zeta potential shows the net charge on the surface of stabilized graphene sheets and represents the degree of dissociation in functional groups of stabilizer. For the Py-SASS-stabilized samples, the zeta potential absolute value decreases with an increase in the concentration of stabilizer. This verifies that the degree of dissociation in the functional group of Py-SASS decreases as the stabilizer concentration increases. At lower stabilizer concentration, the degree

of dissociation in functional group of the stabilizer molecule is higher and adsorption on the graphene surface occurs easily. However, fewer stabilizer molecules are available for adsorption on the graphene surface. An increase in stabilizer concentration provides a higher number of stabilizer molecules, which in turn increases the driving force for stabilizer adsorption on the graphene surface. On the other hand, the degree of dissociation decreases slightly at medium stabilizer concentration. Hence, the net charge on the surface of graphene sheets is slightly lower, but still, it is sufficient to induce strong repulsive forces between graphene sheets. In this condition, more graphene sheets can be stabilized through adsorption of a higher number of stabilizer molecules on graphene sheets. At high stabilizer concentrations, the degree of dissociation in functional groups drops considerably, which alters the dispersion and electrostatic forces in the solution. Although a higher number of stabilizer molecules is available for adsorption, the affinity of the pyrene derivatives for adsorption onto the graphene surface is less. Also, the adsorbed molecules cannot induce strong repulsive forces between graphene sheets and prevent further aggregation of graphene layers.⁴¹ It is less likely that these pyrene derivatives form large structures in the solution or participate in self π – π stacking at higher concentrations,⁴² since the presence of functional groups at short distances from the pyrene basal plane sterically hinders such an arrangement of the molecules.

The most prominent achievement with the pyrene derivatives is the high graphene to stabilizer ratio in the final dispersion, which significantly exceeds other graphene stabilizers such as polymers and surfactants. (Note that higher ratios of graphene to surfactants have been reported; however, lower centrifugation duration and rate in these studies affect dispersion quality.²⁵) A comparison of this ratio for Py-SASS, PVP,

TABLE 1. Comparison of the Effectiveness of Surfactants, Polymers, and Pyrene Derivatives As Stabilizers for Graphene

Stabilizer	Conc. of stabilizer (mg/mL)	Initial Conc. EG (mg/mL)	Final graphene conc. (mg/mL)	Graphene conc. / Stabilizer conc.	Molecular Structure
SDBS	6	50	0.22 ± 0.03	0.036	
PVP	10	50	1 ± 0.1	0.1	
Py-SASS	3	50	1 ± 0.05	0.33	

and SDBS is given in Table 1. The data for PVP and SDBS show the optimal graphene to stabilizer ratio as obtained from our previous studies under the same experimental conditions (Supporting Information).^{28,43} A given graphene dispersion quality can be achieved at far lower mass content of pyrene derivatives than polymers or common surfactants. Therefore, the use of pyrene derivatives as stabilizers improves the dispersion quality for applications in nanocomposites, films, and electronic devices by reducing the amount of undesirable stabilizer molecules present in the product.

The effectiveness of pyrene derivatives for graphene stabilization varied based on the functional group attached to the pyrene. To evaluate the effect of these groups, pyrene derivatives with the same number of sulfonyl, carboxyl, and amine groups were used in the experiments. The results in Figure 3 indicate that Py-SASS is the most effective stabilizer; at its optimum initial concentration, it yields 0.8 mg/mL graphene dispersion. Depending on the sonicator efficiency, the graphene concentration could increase up to 1 mg/mL, which is the highest concentration ever reported for pristine graphene stabilized by pyrene derivatives or surfactants. Higher concentrations reported in the literature were achieved over a long sonication time (24 h) and at lower centrifugation rate (500–1500 rpm) and duration (90 min).⁴⁴ At lower stabilizer concentrations, Py-SASS and Py-SAH with one sulfonyl group yielded the highest concentration of stabilized graphene, while PCA and PBA with carboxyl groups led to lower concentration of graphene. Py-M-NH₂ with an amine group was less effective than other pyrene derivatives. These trends may be explained as follows. The adsorption of pyrene derivative onto the graphene surface occurs through π - π

interactions. The variation of electron density on the pyrene and graphene surface leads to electron donation/acceptance from one surface to the other. Variations in electron density on the aromatic planes may be induced by temporary polarization of the pyrene basal plane, which results in π -electron sharing between graphene and pyrene. Polarization of pyrene occurs in the presence of polar functional groups, which can change the electrons' position in their vicinity. The affinity of graphene layers to share electrons with pyrene depends on the electronegativity of the functional groups. With three atoms of oxygen and a sulfur atom, the sulfonyl group in Py-SASS and Py-SAH has the highest electronegativity relative to the other groups. As a strong electron-withdrawing group, it decreases the electron density on the pyrene basal plane and increases its affinity for accepting electrons from the sp²-hybridized carbon lattice of graphene. Therefore, a higher number of single- to few-layer graphene sheets that were exfoliated by sonication can be stabilized through the adsorption of Py-SASS and Py-SAH. The carboxyl group in PCA and PBA has lower electronegativity due to the presence of a carbon atom instead of a sulfur atom and one less oxygen atom. The lesser electron-withdrawing strength in this group decreases the tendency of graphene to share electrons with pyrene. The amine group has the least electronegativity compared to sulfonyl and carboxyl groups. Thus, it is expected that Py-M-NH₂ will form weaker π - π bonds with graphene sheets (Table S1).

A comparison between Py-SASS- and Py-(SO₃)₄-assisted dispersions is represented in Figure 4. Unexpectedly, an increase in the number of functional groups with high electronegativity yielded a lower graphene concentration in the Py-(SO₃)₄-assisted

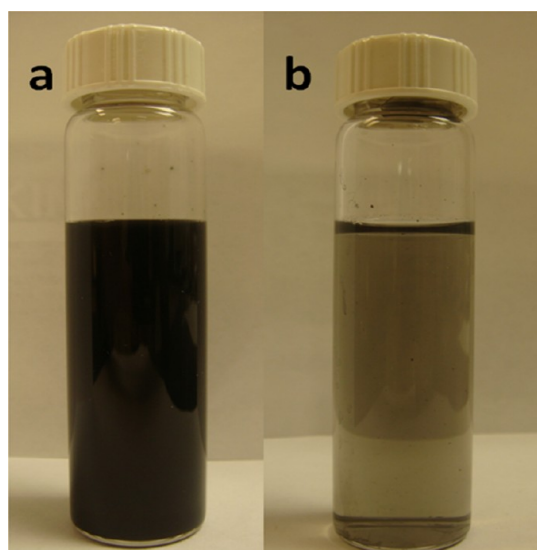


Figure 4. Final concentration of graphene depends on the number of functional groups. (a) Py-SASS-assisted dispersion with final graphene concentration of 0.11 mg/mL and (b) Py-(SO₃)₄-assisted dispersion with final graphene concentration of 0.04 mg/mL. In both samples the concentration of stabilizer is 1 mg/mL.

dispersion. Moreover, the graphene was not stabilized by Py-(SO₃)₄ at concentrations higher than 1 mg/mL of stabilizer. In Py-(SO₃)₄, the symmetric arrangement of functional groups around the basal plane may reduce the probability of temporary polarization. Also, the presence of four functional groups on the basal plane increases the steric hindrance during the adsorption of more Py-(SO₃)₄ molecules on the surface of graphene, which may decrease the surface coverage. Additionally, the dissociation of four sulfonyl groups around the pyrene at low concentrations of stabilizer may cause an accumulation of electrons on the pyrene and reduce its affinity to withdraw electrons from the graphene layers. This decreases the π -electron sharing and the ability of Py-(SO₃)₄ to stabilize graphene in water. At higher concentrations of Py-(SO₃)₄, the concentration of the sulfonyl group rapidly grows since the stabilizer is tetrafunctional. As a result, the dissociation of sulfonyl groups in water becomes less favorable and changes the dispersion and electrostatic forces. In this situation, the minimization of surface free energy may not go through the adsorption path. Instead, complete aggregation occurs, and Py-(SO₃)₄ molecules stay in the aqueous solution.

The distance of the functional groups from the pyrene basal plane is also an important factor. A comparison between PCA- and PBA-assisted dispersion shows how the distance from the pyrene basal plane may affect the final graphene concentration. As the concentration of PCA and PBA increased in the dispersion, PBA was more effective than PCA. As concentration is increased, repulsion forces between negative surface charges increase. In such cases, a longer distance from the basal plane reduces the density of

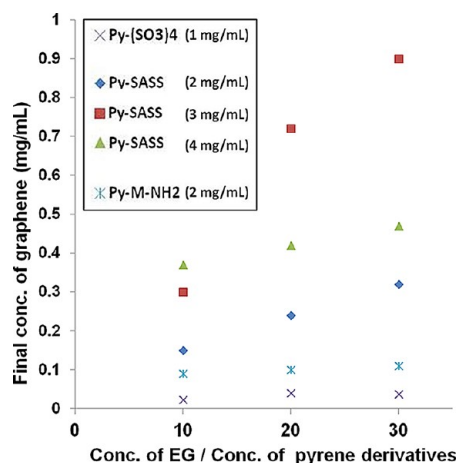


Figure 5. Effect of initial concentration of expanded graphite on final concentration of graphene. Error bars are given in Figure S4.

electrons on the pyrene plane and eases the formation of π - π bonds. This suggests that if the distance of four sulfonyl groups from the pyrene basal plane increases to an optimum value, then the electron density on the pyrene may be optimized in such a way that Py-(SO₃)₄ can stabilize graphene at higher concentrations.

Prior studies have demonstrated that π - π interactions are governed by a combination of dispersion and electrostatic forces in proximity of the graphene/stabilizer.^{45–47} A comparison between Py-SASS and Py-SAH dispersions reveals the effect of electrostatic forces on graphene stabilization since the only difference between these two pyrene derivatives is their counterions. At low concentrations of Py-SASS, the final concentration of graphene was higher than any other sample. This may be attributed to the ionic strength and size of the sodium ion in Py-SASS, which is greater than the ionic strength and size of the hydrogen ion in Py-SAH. The polar functional groups of pyrene derivatives dissociate in the aqueous solution, leaving a layer of counterions on the sides of the graphene sheets. On the basis of DLVO theory, the neutralization of ions occurs at a distance from the surface.⁴⁸ Therefore, a protective layer of counterions with total negative surface charge forms on the graphene layers. This layer acts as a shield that imposes strong electrostatic repulsion forces between ions with the same size and prevents the aggregation of graphene layers. Larger counterions with higher ionic strength cause larger repulsive forces between counterion shields and increase graphene stability.

Figure 5 depicts the effect of initial concentration of expanded graphite on the concentration of graphene in the final dispersion. For all pyrene derivatives investigated, an increase in initial concentration of expanded graphite led to an increase in final concentration of graphene. The presence of more expanded graphite in the solution provides more adsorption sites of pyrene derivatives. However, a large

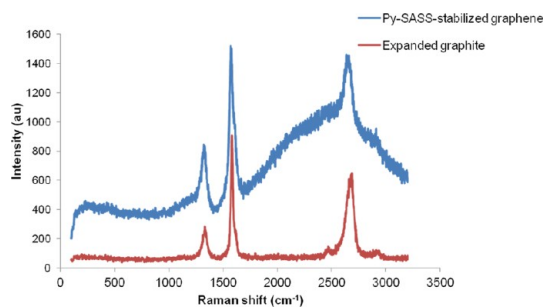


Figure 6. Raman spectra for parent expanded graphite and Py-SASS-stabilized sample. The graphene sample was prepared using 3 mg/mL Py-SASS and 50 mg/mL expanded graphite. The downward shift in 2D band shows the few-layer nature of stabilized graphene. The shoulder seen in the 2D band is due to the presence of Py-SASS on the graphene surface.

amount of expanded graphite may prevent efficient sonication and exfoliation. Moreover, the rate of increase in graphene yield depends on the choice of stabilizer and its initial concentration. For Py-SASS at its optimum initial concentration (3 mg/mL), the rate of increase was significantly higher than in other samples. This suggests that this particular stabilizer effectively absorbs graphene as it becomes available.

Raman spectroscopy was used to evaluate the degree of exfoliation. Figure 6 shows Raman spectra for parent expanded graphite and Py-SASS-stabilized graphene. Both Raman spectra displayed three dominant peaks at about 1330, 1580, and 2680 cm^{-1} , corresponding to the D, G, and 2D band. The G band is representative of sp^2 -hybridized carbon bonds in both graphene and graphite, whereas the D band is representative of either edges or defects in the lattice. This effect is quite weak in graphite. As the graphene flake size decreases during exfoliation, the number of graphene edges exposed per flake increases, which explains the increase in D band intensity in our samples.^{17,49} The 2D band can be used to determine the graphene layer thickness.⁴⁹ The graphene sample shows a downward shift to a lower wavelength, which confirms the few-layer nature of the Py-SASS-stabilized graphene in the dispersion.

TGA was performed to study the thermal stability of the Py-SASS-stabilized graphene, as shown in Figure 7. For TGA analysis the Py-SASS-stabilized dispersion was freeze-dried and washed with the same volume of ethanol to remove the excess stabilizer. The rinsing time was restricted to 2–3 min in order to minimize the possibility of desorption of Py-SASS molecules from the graphene surface. The graphene yielded a 5% mass loss before the furnace temperature reached 500 °C, which is attributed to the evaporation of adsorbed water and residual oxygen-containing groups. The thermal decomposition of Py-SASS occurs at approximately 600 °C, leaving approximately 27% of the mass, which corresponds to the graphene. Thus, the surface coverage of the Py-SASS on the graphene sheets was calculated to be $\sim 3.12 \times 10^{-10}$ mol/ cm^2 . Although the

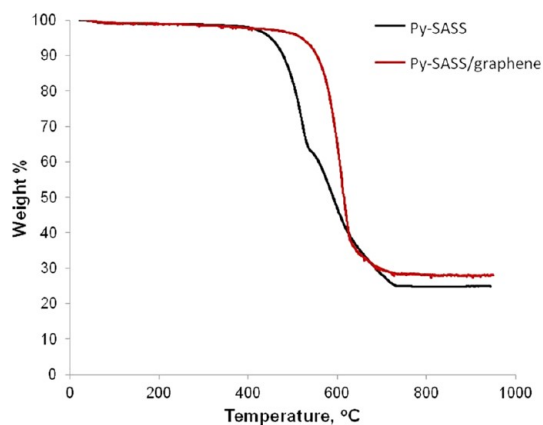


Figure 7. Thermogravimetric analysis of Py-SASS and freeze-dried Py-SASS/graphene powder.

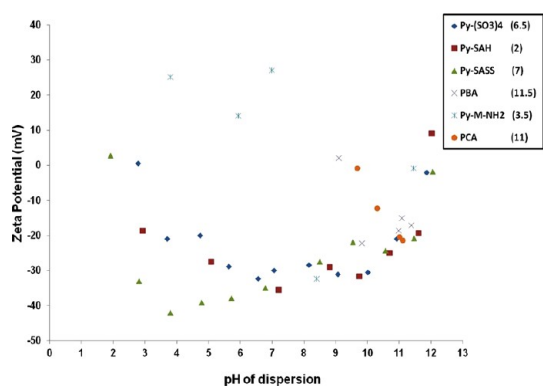


Figure 8. Zeta potential measurements at different pH values of the dispersions. The original pH of each dispersion before any changes is given in parentheses.

sample consisted of single- to few-layer graphene, the calculations were based on a theoretical specific surface area of 2630 m^2/g for single-layer graphene in order to give an approximation of the expected surface coverage. This surface coverage is an order of magnitude higher than the previously reported surface coverage of polymers on the graphene sheets.⁵⁰

Dispersion Stability. All centrifuged dispersions appeared stable for several months, except the Py-SAH-assisted dispersion, which showed signs of aggregation after 2 months. However, to quantify the stability of the dispersions, zeta potential measurements were done; we also investigated the effect of pH on stability. Figure 8 represents the value of the zeta potential for all dispersions at different pH values as well as the original pH of the dispersion. Sulfonyl-containing samples had higher zeta potentials compared to other samples. They were stable over a wide pH range and became unstable solely in extremely acidic or basic media. The Py-SASS- and Py-(SO_3)₄-assisted samples were the most stable dispersions at the original pH of the solution, displaying zeta potentials stronger than ± 30 mV, which is a common stability benchmark. Py-SASS-assisted dispersion actually increases its surface charge as the pH becomes mildly acidic (3.5). However,

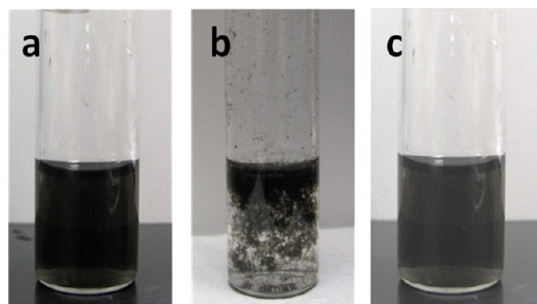


Figure 9. Stability of PCA-stabilized sample against pH changes: (a) The original dispersion at pH = 11, (b) the destabilized dispersion after addition of acid at pH = 3, and (c) the recovered dispersion after increasing the pH to 10.5 by addition of base. (Note that the concentration is lowered simply by dilution effects of the acid and base.)

the Py-SAH sample was not stable at its original, acidic pH. A slight change from the harsh acidic medium to a pH value of 3.8 increased the zeta potential significantly, and at a pH range of 6–8.5, this sample became stable; this explains our earlier observation of aggregation on a long time scale at the original pH. Also, changes in the average particle size of these dispersions are an indicator of graphene sheet aggregation at specific pH values (Table S2). The PCA-, PBA-, and Py-M-NH₂-assisted samples were visibly stable for several months, although measurements showed that they had zeta potentials lower than ± 30 mV at their original pH. Carboxyl groups are efficiently dissociated only in basic media; so, the PCA- and PBA-assisted dispersions were destabilized by a slight decrease in pH. The Py-M-NH₂-assisted dispersion was the only sample with a positive surface charge, and its zeta potential value did not change upon pH decrease. However, it immediately destabilized at higher pH values due to a reduction in amine group dissociation in basic conditions.

Furthermore, it was possible to restabilize graphene in the dispersion by addition of NaOH to recover the original pH of the dispersion in PCA- and PBA-assisted dispersions. Figure 9 shows the destabilization and recovery of the PCA-assisted dispersion. This observation proves that pH changes do not affect the adsorption of stabilizer on the graphene layer; instead, pH changes simply increase/decrease the dissociation degree of functional groups and hydrogen bonding between functional groups and the solvent. This in turn impacts the electrostatic forces on the graphene surface and results in further stabilization/destabilization of adsorbed PCA and PBA molecules on the graphene surface. Thus, the destabilization of PCA- and PBA-assisted dispersions after decreasing the pH is a reversible flocculation process rather than desorption of stabilizer molecules from the graphene surface, which leads to an irreversible agglomeration of the particles.

Dispersion stability was also tested by redispersion of the samples after lyophilization. After centrifugation, the dispersions were freeze-dried to yield a dark gray powder, which was then redispersed in the same amount

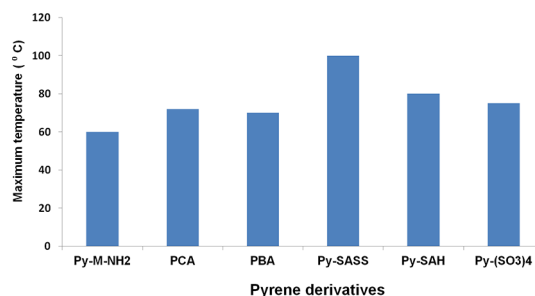


Figure 10. Apparent stability of the dispersions at high temperatures. At temperatures above those in this graph, the samples visibly aggregated. Error bars are given in the Supporting Information (Figure S5).

of water. In the case of sulfonyl functional groups in Py-SASS- and Py-SAH-assisted dispersions, the freeze-dried powder was easily redispersible without any need for sonication. In all other samples, partial sedimentation of graphene was observed after centrifugation.

The visible stability of dispersions against increases in temperature is depicted in Figure 10. The Py-SASS-assisted dispersions were stable up to 100 °C. Dispersions containing sulfonyl groups were stable up to higher temperatures than stabilizers with other functional groups. This might be attributed to their stronger interactions with the graphene surface. Stability at higher temperatures makes these dispersions promising for applications in nanocomposites and electronic devices.

Solvent Effects. In addition to water, other organic solvents, i.e., ethanol, methanol, and acetone, were also investigated in this study. However, graphene sheets were stabilized only in aqueous solution, and any attempt to disperse graphene in other solvents led to immediate sedimentation of graphite after sonication. This may be attributed to the difference between the polarity and surface free energy of water and those of other solvents used in this study. The driving force for stabilizer adsorption occurs if the difference in polarity between the stabilizer and the solvent is sufficiently large. This effect is much stronger in water than other solvents; in water, the pyrene basal plane minimizes its free energy by adsorbing to the graphene surface. Ethanol, methanol, and acetone have lower polarity and surface energies and do not induce adsorption of the pyrene basal plane. Without sufficient stabilizer adsorption, the graphene simply aggregates.

The concentration of graphene after addition of ethanol to the Py-SASS-assisted dispersion and centrifugation is represented in Figure 11. The pH of the dispersion gradually changed from 6.6 in the original dispersion to 7.2 in the presence of a 90 vol % of ethanol. The graphene concentration decreased considerably by addition of ethanol after 1 h centrifugation. The presence of ethanol in the dispersion changes the polarity of the solution and also the difference between the polarity of Py-SASS and solvent. This leads to desorption of some Py-SASS molecules from the

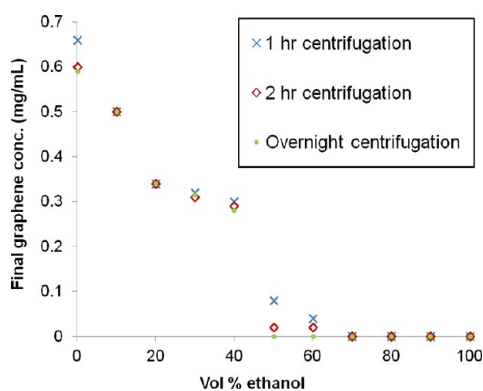


Figure 11. Final concentration of graphene as a function of vol % of ethanol and centrifugation time. Ethanol was added to an aqueous dispersion of graphene to prepare dispersions containing 10 to 90 vol % ethanol.

surface of the graphene sheets. At a lower concentration of Py-SASS molecules on the surface, the repulsive forces between graphene layers are weak, and aggregation ensues. When the amount of ethanol in the dispersion exceeded 60 vol %, the polarity of dispersion changed in such a way that most of the Py-SASS molecules desorbed from the graphene layers during the first hour of centrifugation, and complete aggregation of graphene sheets occurred. Further centrifugation for another 1 h led to complete aggregation of graphene sheets in samples containing 50 and 60 vol % ethanol. This observation verifies that desorption of Py-SASS molecules from the surface of graphene sheets is a transition between two equilibrium states, which is a time-dependent process. The graphene concentration in samples containing 10–40 vol % did not change with overnight centrifugation, indicating that the contribution of up to 40 vol % of ethanol in the dispersion medium allows the adsorption of a limited number of Py-SASS molecules, which is required for graphene stabilization.

Polymer Nanocomposites. Prior applications of pyrene derivative-stabilized graphene have focused on chemical sensors.³⁴ We investigated the applicability of these dispersions in polymer composites for the first time. The preparation procedure and results are explained in the Supporting Information. Electrically conductive graphene/epoxy composites were prepared using the Py-SASS-stabilized graphene (Figure S6). SEM images of these composite are represented in Figure S7. The compatibility of Py-SASS- and Py-SAH-stabilized dispersions with an epoxy matrix resulted in a successful preparation of a conductive graphene/epoxy composite. In contrast, graphene dispersed by SDBS (a common conventional surfactant) was not

compatible with the epoxy matrix. The presence of large amounts of SDBS, which might not be compatible with epoxy, can cause a phase separation during the preparation. These results showed the advantage of stackers over surfactants when used as stabilizer in graphene dispersions. Dispersed graphene sheets in the epoxy matrix are shown in Figure S8. Also, the electrical conductivity and mechanical properties (Table S3) of this sample were comparable with the previous results obtained by our group for PVP-stabilized graphene/epoxy composite.^{28,51}

CONCLUSION

We used various pyrene derivatives to stabilize high concentrations of graphene sheets in aqueous dispersions, which were stable for several months. Among all our pyrene derivatives, Py-SASS was the most effective one, yielding graphene final concentrations as high as 0.8–1 mg/mL. The most notable achievement with pyrene derivatives was the graphene to stabilizer yield obtained in the dispersions, which significantly exceeds this value in polymer- and surfactant-stabilized samples. We found that a sufficient difference between the polarity of the solvent and the stabilizer is required for adsorption onto the graphene surface. We also investigated the role of functional groups of pyrene derivatives in the stabilization process and that the functional groups with higher electronegativity are more efficient in driving the adsorption of stabilizers onto the graphene layers. At the same time, the number of functional groups, their arrangement around the pyrene basal plane, and their distances from the pyrene molecule should be optimized to give the highest number of adsorbed molecules and stabilized graphene. Zeta potential measurements showed that pyrene derivatives with sulfonyl groups produce the most stable dispersion over a wide range of pH. However, pyrene derivatives with carboxyl and amine groups were stable at specific pH values, and a slight change from the original pH caused destabilization in their dispersions. Finally, we prepared graphene/epoxy composites using this dispersion and compared them with PVP-stabilized graphene/epoxy composites. Similar mechanical and electrical properties were obtained for both types of samples, while significantly less stabilizer was used in the present case. By knowing the effect of each parameter in the stabilization of graphene, we may design ideal graphene stabilizers by manipulating the molecular structures in order to obtain graphene dispersions with high quality.

MATERIALS AND METHODS

Materials. Expanded graphite was provided by Asbury Carbons (CAS# 7782-42-5, grade 3805). The stabilizers, pyrene, 1-aminopyrene (Py-NH₂), 1-pyrenemethylamine hydrochloride

(Py-M-NH₂), 1-pyrenecarboxylic acid (PCA), 1-pyrenebutyric acid (PBA), 1-pyrenebutanol, 1-pyrenesulfonic acid hydrate (Py-SAH), 1-pyrenesulfonic acid sodium salt (Py-SASS), and 1,3,6,8-pyrenetetrasulfonic acid tetra sodium salt (Py-(SO₃)₄),

were purchased from Sigma-Aldrich. Polyvinylpyrrolidone (PVP) with $M_w \sim 10\,000$ was purchased from Sigma-Aldrich. Sodium dodecylbenzenesulfonate (SDBS) was purchased from MP Bio-medicals. All the chemicals were used as received.

Preparation of Graphene Dispersions. Pyrene derivatives with various functional groups were used as stabilizers. In a typical preparation, a specific amount of stabilizer was added to 20 mL of deionized water (DI) and stirred at 80 °C to obtain a clear solution of stabilizer in water. When PCA and PBA were used as stabilizer, the pH of the solution was increased to 10 by addition of ammonium hydroxide in order to dissolve them in DI water. Expanded graphite (EG) was added to this solution and tip sonicated for 1 h using a Misonix sonicator (XL 2000) at an output wattage of 7W at room temperature. During the sonication the temperature was kept at room temperature using an ice bath in order to maintain the efficiency of exfoliation. The dispersion was then centrifuged (Centrifuge 225, Fischer Scientific) at 5000 rpm for 4 h to remove larger aggregates, and the supernatant was collected. This stable dispersion was used for further characterizations and composite production. The initial concentration of stabilizer was different for each stabilizer and varied from 0.5 to 7 mg/mL in this study. The ratio of the initial concentration of EG to initial concentration of stabilizer was 10, 20, and 30 in order to study the effect of concentration of EG on dispersion. The exact amount of pyrene derivatives and the ratio of pyrene derivatives to graphite are given as data points in Figure 3 and Figure 5. Graphene dispersions were prepared by the same procedure using PVP and SDBS as stabilizers to compare the effectiveness of pyrene derivatives against other types of stabilizers. The initial concentration of SDBS and PVP was 6 and 10 mg/mL, respectively.

Characterization of Graphene Dispersion. UV–vis spectroscopy was performed on a Shimadzu UV–vis spectrophotometer 2550 at a wavelength of 660 nm on the liquid samples to measure the concentration of the graphene in dispersion. To eliminate the effects of the stabilizer solution, the absorbance was measured against the stabilizer solution. The concentration was determined using Beer's law. Vacuum filtration was used to calculate the extinction coefficient of stabilizer solution in water. A regular vacuum filtration setup was utilized to measure the concentration of graphene in the dispersion. A polytetrafluoroethylene filter paper with a pore size of 0.02 μm was used. The mass of the filter paper before and after filtration was measured and used to determine the concentration of graphene. The same filtered samples were used to measure Raman spectra on a Renishaw Raman microscope using a 633 nm He–Ne laser.

High-resolution transmission electron microscopy (HRTEM) samples were prepared by deposition of liquid samples on 400 mesh carbon-coated copper grids (Electron Microscopy Sciences, CF400-Cu) and air drying for 1 min. A voltage of 75 kV was used to image the samples on a Hitachi H8100.

Thermogravimetric analysis (TGA) was carried out in a TGA i 1000 (Instrument Specialist Inc.). The temperature was raised from 0 °C to 1000 °C at the rate of 10 °C/min.

Zeta potential measurements were conducted on a Zetatracs analyzer from Microtrac Inc. Two laser beams at 780 nm were irradiated to measure the electrophoretic mobility of particles using the principles of dynamic light scattering. The Zetatracs analyzer calculates the value of the zeta potential from electrophoretic mobility using the Smoluchowski equation: $\xi = \mu\eta/\epsilon$, where ξ is the zeta potential, μ is the mobility, η is the viscosity of the solution, and ϵ is the dielectric constant of the solvent. Also, the variation of zeta potential against pH changes was assessed for Py-SASS-, Py-SAH-, Py-(SO₃)₄-, Py-M-NH₂-, PCA-, and PBA-stabilized dispersions. For these experiments the original pH of dispersion was changed by dropwise addition of hydrochloric acid (HCl) and sodium hydroxide (NaOH) to the dispersions in an autotitrator from Microtrac Inc. All measurements were conducted at room temperature.

Dispersion Stability Tests. Graphene dispersions were frozen in a freezer at –20 °C and further dried in a freeze-dryer (Vitriscan benchtop freeze-dryer) overnight to yield dry powdered samples. The freeze-dried samples were redispersed in water and sonicated for 5 min. Redispersed samples were centrifuged, and the concentration of graphene in the supernatant was

measured to evaluate the redispersibility of the graphene. Visible stability of the dispersion at higher temperatures was tested by heating and centrifugation of the dispersions. Samples were heated gradually, and after each 10 °C raise in the temperature they were centrifuged for 30 min to check the possibility of visible sedimentation at higher temperatures. Above 70 °C, samples were centrifuged after each 5 °C raise in the temperature.

Desorption of Py-SASS from the graphene surface in the presence of ethanol was studied by adding ethanol to Py-SASS-assisted dispersions to get dispersions with 10–90 vol % of ethanol. All samples were centrifuged simultaneously for 1 h, and then the concentration of graphene in the supernatant was measured to study desorption of Py-SASS from graphene in the presence of ethanol. Samples containing graphene in the supernatant were centrifuged for another 1 h to test the time dependence of the desorption process.

Conflict of Interest: The authors declare no competing financial interest.

Acknowledgment. We appreciate helpful insight from Ahmed Wajid, Robert Fullerton, Abel Cortinas, Ronald Hedden, Alan Jankowski, and Dominick Casadonte of Texas Tech University. TEM was performed at the TTU Imaging Center (funded by NSF MRI 04-511) supported by Dr. Mark J. Grimson and Prof. Lauren S. Gollahon. Zeta potential measurements were performed in the Materials Characterization Center with the support of Dr. Juliusz Warzywoda, Dr. Louisa Hope-Weeks, and Dr. Al Sacco of TTU. We acknowledge Colin Young and Prof. Matteo Pasquali of Rice University for their help with the Raman measurements. We also acknowledge DSC assistance from Dr. Brandon Weeks of TTU. Funding was provided by the U.S. National Science Foundation (NSF) under award CBET-1032330 and by the Air Force Office of Scientific Research Young Investigator Program (AFOSR FA9550-11-1-0027). A portion of this research was conducted at the Center for Nanophase Materials Sciences, which is sponsored at Oak Ridge National Laboratory by the Office of Basic Energy Sciences, U.S. Department of Energy (CNMS User Nanoscience Research Program 2011-230).

Supporting Information Available: Additional TEM images of graphene sheets (Figure S1), the error bars for the graph showing stabilizer concentration, graphite concentration, and stability against temperature (Figures S2, S4, and S5), the zeta potential changes with Py-SASS concentration (Figure S3), effect of functional groups on graphene yield (Table S1), particle size measurements (Table S2), preparation of graphene/epoxy composite (Figure S6), SEM images of composite (Figure S7), electrical and mechanical properties of composite (Table S3), and dispersion of graphene in epoxy (Figure S8). This material is available free of charge via the Internet at <http://pubs.acs.org>.

REFERENCES AND NOTES

- Geim, A. K.; Novoselov, K. S. The Rise of Graphene. *Nat. Mater.* **2007**, *6*, 183–191.
- Novoselov, K. S.; Jiang, D.; Schedin, F.; Booth, T. J.; Khotkevich, V. V.; Morozov, S. V.; Geim, A. K. Two-Dimensional Atomic Crystals. *Proc. Natl. Acad. Sci. U. S. A.* **2005**, *102*, 10451–10453.
- Kim, H.; Macosko, C. W. Morphology and Properties of Polyester/Exfoliated Graphite Nanocomposites. *Macromolecules* **2008**, *41*, 3317–3327.
- Ansari, S.; Giannelis, E. P. Functionalized Graphene Sheet-Poly(vinylidene fluoride) Conductive Nanocomposites. *J. Polym. Sci., Part B: Polym. Phys.* **2009**, *47*, 888–897.
- Eda, G.; Chowalla, M. Graphene-Based Composite Thin Films for Electronics. *Nano Lett.* **2009**, *9*, 814–818.
- Li, D.; Mueller, M. B.; Gilje, S.; Kaner, R. B.; Wallace, G. G. Processable Aqueous Dispersions of Graphene Nanosheets. *Nat. Nanotechnol.* **2008**, *3*, 101–105.
- Worsley, M. A.; Pauzaskie, P. J.; Kucheyev, S. O.; Zaig, J. M.; Hamza, A. V.; Satcher, J. H., Jr.; Baumann, T. F. Properties of Single-Walled Carbon Nanotube-Based Aerogels as a Function of Nanotube Loading. *Acta Mater.* **2009**, *57*, 5131–5136.

8. Worsley, M. A.; Pauzauskie, P. J.; Olson, T. Y.; Biener, J.; Satcher, J. H., Jr.; Baumann, T. F. Synthesis of Graphene Aerogel with High Electrical Conductivity. *J. Am. Chem. Soc.* **2010**, *132*, 14067–14069.
9. Liu, Q.; Liu, Z.; Zhong, X.; Yang, L.; Zhang, N.; Pan, G.; Yin, S.; Chen, Y.; Wei, J. Polymer Photovoltaic Cells Based on Solution-Processable Graphene and P3HT. *Adv. Funct. Mater.* **2009**, *19*, 894–904.
10. Liu, Z.; He, D.; Wang, Y.; Wu, H.; Wang, J.; Wang, H. Improving Photovoltaic Properties by Incorporating Both Single Walled Carbon Nanotubes and Functionalized Multiwalled Carbon Nanotubes. *Sol. Energy Mater. Sol. Cells* **2010**, *94*, 2148–2153.
11. Liu, Z.; Liu, Q.; Huang, Y.; Ma, Y.; Yin, S.; Zhang, X.; Sun, W.; Chen, Y. Organic Photovoltaic Devices Based on a Novel Acceptor Material: Graphene. *Adv. Mater.* **2008**, *20*, 3924+.
12. Huang, L.; Huang, Y.; Liang, J.; Wan, X.; Chen, Y. Graphene-Based Conducting Inks for Direct Inkjet Printing of Flexible Conductive Patterns and Their Applications in Electric Circuits and Chemical Sensors. *Nano Res.* **2011**, *4*, 675–684.
13. Shin, K.-Y.; Hong, J.-Y.; Jang, J. Flexible and Transparent Graphene Films as Acoustic Actuator Electrodes Using Inkjet Printing. *Chem. Commun.* **2011**, *47*, 8527–8529.
14. Sriprachubwong, C.; Karuwan, C.; Wisitsorrat, A.; Phokharatkul, D.; Lomas, T.; Sritongkham, P.; Tuantranont, A. Inkjet-Printed Graphene-PEDOT:PSS Modified Screen Printed Carbon Electrode for Biochemical Sensing. *J. Mater. Chem.* **2012**, *22*, 5478–5485.
15. Park, S.; Ruoff, R. S. Chemical Methods for the Production of Graphenes. *Nat. Nanotechnol.* **2009**, *4*, 217–224.
16. Israelachvili, J. N. *Intermolecular and Surface Forces*, 2nd ed.; Academic Press: New York, 1991.
17. Behabtu, N.; Lomeda, J. R.; Green, M. J.; Higginbotham, A. L.; Sinitskii, A.; Kosynkin, D. V.; Tsentlovich, D.; Parras-Vasquez, A. N. G.; Schmidt, J.; Kesselman, E.; *et al.* Spontaneous High-Concentration Dispersions and Liquid Crystals of Graphene. *Nat. Nanotechnol.* **2010**, *5*.
18. Park, S.; An, J.; Jung, I.; Piner, R. D.; An, S. J.; Li, X.; Velamakanni, A.; Ruoff, R. S. Colloidal Suspensions of Highly Reduced Graphene Oxide in a Wide Variety of Organic Solvents. *Nano Lett.* **2009**, *9*, 1593–1597.
19. Stankovich, S.; Dikin, D. A.; Piner, R. D.; Kohlhaas, K. A.; Kleinhammes, A.; Jia, Y.; Wu, Y.; Nguyen, S. T.; Ruoff, R. S. Synthesis of Graphene-Based Nanosheets via Chemical Reduction of Exfoliated Graphite Oxide. *Carbon* **2007**, *45*, 1558–1565.
20. Tung, V. C.; Allen, M. J.; Yang, Y.; Kaner, R. B. High-Throughput Solution Processing of Large-Scale Graphene. *Nat. Nanotechnol.* **2009**, *4*, 25–29.
21. Eda, G.; Fanchini, G.; Chhowalla, M. Large-Area Ultrathin Films of Reduced Graphene Oxide as a Transparent and Flexible Electronic Material. *Nat. Nanotechnol.* **2008**, *3*, 270–274.
22. Rourke, J. P.; Pandey, P. A.; Moore, J. J.; Bates, M.; Kinloch, I. A.; Young, R. J.; Wilson, N. R. The Real Graphene Oxide Revealed: Stripping the Oxidative Debris from the Graphene-like Sheets. *Angew. Chem., Int. Ed.* **2011**, *50*, 3173–3177.
23. Dreyer, D. R.; Park, S.; Bielawski, C. W.; Ruoff, R. S. The Chemistry of Graphene Oxide. *Chem. Soc. Rev.* **2010**, *39*.
24. Green, A. A.; Hersam, M. C. Solution Phase Production of Graphene with Controlled Thickness via Density Differentiation. *Nano Lett.* **2009**, *9*, 4031–4036.
25. Lotya, M.; King, P. J.; Khan, U.; De, S.; Coleman, J. N. High-Concentration, Surfactant-Stabilized Graphene Dispersions. *ACS Nano* **2010**, *4*, 3155–3162.
26. De, S.; King, P. J.; Lotya, M.; O'Neill, A.; Doherty, E. M.; Hernandez, Y.; Duesberg, G. S.; Coleman, J. N. Flexible, Transparent, Conducting Films of Randomly Stacked Graphene from Surfactant-Stabilized, Oxide-Free Graphene Dispersions. *Small* **2010**, *6*, 458–464.
27. Vadukumpully, S.; Paul, J.; Valiyaveetil, S. Cationic Surfactant Mediated Exfoliation of Graphite into Graphene Flakes. *Carbon* **2009**, *47*, 3288–3294.
28. Wajid, A. S.; Das, S.; Irin, F.; Ahmed, H. S. T.; Shelburne, J. L.; Parviz, D.; Fullerton, R. J.; Jankowski, A. F.; Hedden, R. C.; Green, M. J. Polymer-Stabilized Graphene Dispersions at High Concentrations in Organic Solvents for Composite Production. *Carbon* **2012**, *50*, 526–534.
29. Bourlino, A. B.; Georgakilas, V.; Zboril, R.; Steriotis, T. A.; Stubos, A. K.; Trapalis, C. Aqueous-Phase Exfoliation of Graphite in the Presence of Polyvinylpyrrolidone for the Production of Water-Soluble Graphenes. *Solid State Commun.* **2009**, *149*, 2172–2176.
30. Das, S.; Irin, F.; Tanvir Ahmed, H. S.; Cortinas, A. B.; Wajid, A. S.; Parviz, D.; Jankowski, A. F.; Kato, M.; Green, M. J. Non-Covalent Functionalization of Pristine Few-Layer Graphene Using Triphenylene Derivatives for Conductive Poly (Vinyl Alcohol) Composites. *Polymer* **2012**, *53*, 2485–2494.
31. Guardia, L.; Fernandez-Merino, M. J.; Paredes, J. I.; Solis-Fernandez, P.; Villar-Rodil, S.; Martinez-Alonso, A.; Tascon, J. M. D. High-Throughput Production of Pristine Graphene in an Aqueous Dispersion Assisted by Non-Ionic Surfactants. *Carbon* **2011**, *49*, 1653–1662.
32. Chen, Z.; Lohr, A.; Saha-Moeller, C. R.; Wuerthner, F. Self-Assembled Pi-Stacks of Functional Dyes in Solution: Structural and Thermodynamic Features. *Chem. Soc. Rev.* **2009**, *38*, 564–584.
33. Fujigaya, T.; Nakashima, N. Methodology for Homogeneous Dispersion of Single-Walled Carbon Nanotubes by Physical Modification. *Polym. J.* **2008**, *40*, 577–589.
34. An, X.; Simmons, T. J.; Shah, R.; Wolfe, C.; Lewis, K. M.; Washington, M.; Nayak, S. K.; Talapatra, S.; Kar, S. Stable Aqueous Dispersions of Noncovalently Functionalized Graphene from Graphite and Their Multifunctional High-Performance Applications. *Nano Lett.* **2010**, *10*, 4295–4301.
35. Zhang, M.; Parajuli, R. R.; Mastrogianni, D.; Dai, B.; Lo, P.; Cheung, W.; Brukh, R.; Chiu, P. L.; Zhou, T.; Liu, Z.; *et al.* Production of Graphene Sheets by Direct Dispersion with Aromatic Healing Agents. *Small* **2010**, *6*, 1100–1107.
36. Xu, Y.; Bai, H.; Lu, G.; Li, C.; Shi, G. Flexible Graphene Films via the Filtration of Water-Soluble Noncovalent Functionalized Graphene Sheets. *J. Am. Chem. Soc.* **2008**, *130*, 5856+.
37. Su, Q.; Pang, S.; Alijani, V.; Li, C.; Feng, X.; Muellen, K. Composites of Graphene with Large Aromatic Molecules. *Adv. Mater.* **2009**, *21*, 3191+.
38. Jang, J.-H.; Rangappa, D.; Kwon, Y.-U.; Honma, I. Direct Preparation of 1-PSA Modified Graphene Nanosheets by Supercritical Fluidic Exfoliation and its Electrochemical Properties. *J. Mater. Chem.* **2011**, *21*, 3462–3466.
39. Lotya, M.; Hernandez, Y.; King, P. J.; Smith, R. J.; Nicolosi, V.; Karlsson, L. S.; Blighe, F. M.; De, S.; Wang, Z. M.; McGovern, I. T.; *et al.* Liquid Phase Production of Graphene by Exfoliation of Graphite in Surfactant/Water Solutions. *J. Am. Chem. Soc.* **2009**, *131*, 3611–3620.
40. Behabtu, N.; Lomeda, J. R.; Green, M. J.; Higginbotham, A. L.; Sinitskii, A.; Kosynkin, D. V.; Tsentlovich, D.; Parras-Vasquez, A. N. G.; Schmidt, J.; Kesselman, E.; *et al.* Spontaneous High-Concentration Dispersions and Liquid Crystals of Graphene. *Nat. Nanotechnol.* **2010**, *5*, 406–411.
41. Vigolo, B.; Penicaud, A.; Coulon, C.; Sauder, C.; Pailler, R.; Journet, C.; Bernier, P.; Poulin, P. Macroscopic Fibers and Ribbons of Oriented Carbon Nanotubes. *Science* **2000**, *290*.
42. Ebel, A.; Donaubauer, W.; Hampel, F.; Hirsch, A. Amphiphilic Pyrene-Functionalized Dendrons: Synthesis and Intermolecular Interactions. *Eur. J. Org. Chem.* **2007**, 3488–3494.
43. Das, S.; Wajid, A. S.; Shelburne, J. L.; Liao, Y.-C.; Green, M. J. Localized In Situ Polymerization on Graphene Surfaces for Stabilized Graphene Dispersions. *ACS Appl. Mater. Interfaces* **2011**, *3*.
44. Sun, Z.; Masa, J.; Liu, Z.; Schuhmann, W.; Muhler, M. Highly Concentrated Aqueous Dispersions of Graphene Exfoliated by Sodium Taurodeoxycholate: Dispersion Behavior and Potential Application as a Catalyst Support for the Oxygen-Reduction Reaction. *Chem.—Eur. J.* **2012**, *18*.

45. Bjoerk, J.; Hanke, F.; Palma, C.-A.; Samori, P.; Cecchini, M.; Persson, M. Adsorption of Aromatic and Anti-Aromatic Systems on Graphene through Pi-Pi Stacking. *J. Phys. Chem. Lett.* **2010**, *1*, 3407–3412.
46. Ershova, O. V.; Lillestolen, T. C.; Bichoutskaia, E. Study of Polycyclic Aromatic Hydrocarbons Adsorbed on Graphene Using Density Functional Theory with Empirical Dispersion Correction. *Phys. Chem. Chem. Phys.* **2010**, *12*, 6483–6491.
47. Feng, C.; Lin, C. S.; Fan, W.; Zhang, R. Q.; Van Hove, M. A. Stacking of Polycyclic Aromatic Hydrocarbons as Prototype for Graphene Multilayers, Studied Using Density Functional Theory Augmented with a Dispersion Term. *J. Chem. Phys.* **2009**, 131.
48. Hunter, R. J. *Zeta Potential in Colloid Science: Principles and Applications*, 2nd ed.; Academic Press: New York, 1981.
49. Ferrari, A. C.; Meyer, J. C.; Scardaci, V.; Casiraghi, C.; Lazzeri, M.; Mauri, F.; Piscanec, S.; Jiang, D.; Novoselov, K. S.; Roth, S.; Geim, A. K. Raman Spectrum of Graphene and Graphene Layers. *Phys. Rev. Lett.* **2006**, 97.
50. Liu, J.; Yang, W.; Tao, L.; Li, D.; Boyer, C.; Davis, T. P. Thermosensitive Graphene Nanocomposites Formed Using Pyrene-Terminal Polymers Made by RAFT Polymerization. *J. Polym. Sci., Part A: Polym. Chem.* **2010**, *48*, 425–433.
51. Wajid, A. S.; Ahmed, H. S. T.; Das, S.; Irin, F.; Jankowski, A. F.; Green, M. J. High-Performance Pristine Graphene/Epoxy Composites with Enhanced Mechanical and Electrical Properties. *Macromol. Mater. Eng.* **2012**, in press, DOI 10.1002/mame.201200043.